



Mixing state and sources of submicron regional background aerosols in the northern Qinghai–Tibet Plateau and the influence of biomass burning

W. J. Li¹, S. R. Chen¹, Y. S. Xu², X. C. Guo^{1,2}, Y. L. Sun³, X. Y. Yang², Z. F. Wang³, X. D. Zhao⁴, J. M. Chen¹, and W. X. Wang^{1,2}

¹Environment Research Institute, Shandong University, 250100, Jinan, China

²Chinese Research Academy of Environmental Sciences, Beijing 100012, China

³State Key Laboratory of Atmospheric Boundary Layer Physics and Atmospheric Chemistry, Institute of Atmospheric Physics, Chinese Academy of Sciences, Beijing 100029, China

⁴Qinghai Environmental Monitoring Center, Qinghai 810007, China

Correspondence to: W. J. Li (liweijun@sdu.edu.cn) and J. M. Chen (jmchen@sdu.edu.cn)

Received: 16 June 2015 – Published in Atmos. Chem. Phys. Discuss.: 8 September 2015

Revised: 4 November 2015 – Accepted: 14 November 2015 – Published: 2 December 2015

Abstract. Transmission electron microscopy (TEM) was employed to obtain morphology, size, composition, and mixing state of background aerosols with diameter less than 1 μm in the northern Qinghai–Tibet Plateau (QTP) during 15 September to 15 October 2013. Individual aerosol particles mainly contained secondary inorganic aerosols (SIA – sulfate and nitrate) and organics during clean periods ($\text{PM}_{2.5}$ mass concentration less than $2.5 \mu\text{g m}^{-3}$). The presence of K–Na–Cl associated with organics and an increase in soot particles suggest that an intense biomass burning event caused the highest $\text{PM}_{2.5}$ concentrations ($> 30 \mu\text{g m}^{-3}$) during the study. A large number fraction of the fly-ash-containing particles (21.73 %) suggests that coal combustion emissions in the QTP significantly contributed to air pollutants at the medium pollution level ($\text{PM}_{2.5}$: $10\text{--}30 \mu\text{g m}^{-3}$). We concluded that emissions from biomass burning and from coal combustion both constantly contribute to anthropogenic particles in the QTP atmosphere. Based on size distributions of individual particles at different pollution levels, we found that gas condensation on existing particles is an important chemical process for the formation of SIA with organic coating. TEM observations show that refractory aerosols (e.g., soot, fly ash, and visible organic particles) likely adhere to the surface of SIA particles larger than 200 nm due to coagulation. Organic coating and soot on surface of the aged particles likely influence their hygroscopic and optical prop-

erties, respectively, in the QTP. To our knowledge, this study reports the first microscopic analysis of fine particles in the background QTP air.

1 Introduction

With an immense area (about 2 400 000 km^2) and mean elevation of more than 4000 m a.s.l., the Tibetan Plateau (TP), often referred to as the “ridge of the world” or the “third pole”, plays a key role in Asian climatology, especially the formation of monsoons (Lau et al., 2006). Climate on the TP has warmed 0.3 °C per decade over the past three decades, which is twice the rate of observed global warming (Xu et al., 2009). Anthropogenic aerosols and their ice and cloud condensation nuclei (CCN) directly or indirectly led to the brightening and dimming phenomenon before and after the 1980s in the TP (You et al., 2010). However, light-absorbing carbonaceous aerosol particles (i.e., black carbon (BC) and brown carbon (BrC)) can warm the troposphere (Ramanathan and Carmichael, 2008) and accelerate glacier retreat (Xu et al., 2009). Both the radiative effects of aerosols and their role in cloud forming processes depend on their number, size, chemical properties, and mixing state.

As a consequence, a better understanding of climate change can be achieved by characterizing the TP aerosols.

Many aerosol measurements have been conducted in the TP. Ion composition records from a shallow ice core (Zheng et al., 2010) and black soot in the Tibetan glaciers (Xu et al., 2009) both showed that anthropogenic aerosols have increased significantly in the most recent 50 years in the TP. J. J. Li et al. (2013) obtained aerosol components such as 61 % mineral dust, 3 % ammonium, 4 % nitrate, 18 % sulfate, 2 % black carbon, and 12 % organic matter in $PM_{2.5}$ at a concentration of $21.5 \mu\text{g m}^{-3}$ during summer of 2010 at Qinghai Lake ($36^{\circ}59' \text{N}$, $99^{\circ}54' \text{E}$; 3200 m a.s.l.) in the northeastern part of the TP. Coal burning and biomass burning were the major sources for anthropogenic aerosols. Xu et al. (2014) showed that the $PM_{2.5}$ mass concentration of $9.5 \pm 5.4 \mu\text{g m}^{-3}$ during a year-long study at the Qilian Shan Station (39.50°N , 96.51°E ; 4180 m a.s.l.), a remote site on the northeast edge of the Tibetan Plateau, and their water-soluble ionic species were dominated by SO_4^{2-} (39 %), CO_3^{2-} (19 %), Ca^{2+} (16 %), NO_3^- (10 %), and NH_4^+ (6 %). Their study suggests that anthropogenic aerosol and natural mineral dust from the Gobi desert together contribute to the particle loading in this remote air. Li et al. (2007) also found anthropogenic ions from residential combustion emissions in precipitation samples at Nam Co station of the central TP. In addition, long-range transport of pollutants from eastern and northwestern China and northern India can contribute black carbon and other air pollutants to the TP region (Cao et al., 2010; Wang et al., 2010; Engling et al., 2011; Kopacz et al., 2011; Lu et al., 2012; Xu et al., 2013; Zhao et al., 2013; Cong et al., 2015; Duo et al., 2015). Although anthropogenic sources make but a minor contribution to the background TP atmosphere, these anthropogenic aerosols significantly enhanced aerosol optical properties in the central and northeastern TP in summer (Cong et al., 2009b; Che et al., 2011; Xia et al., 2011). Therefore, study of the composition and sources of aerosol particles in the TP is necessary to understand their effects on the optical, CCN, or IN activity.

The TP has various geographic and natural environmental ecosystems such as mountains, lake basins, deserts, forests, and grasslands. Previous sampling sites have included mountain forests, lake basins, and urban areas in the TP (Li et al., 2007; Che et al., 2011; Engling et al., 2011; J. J. Li et al., 2013; Xu et al., 2014). Grassland is one of the largest landscapes in the TP. There are only a few herdsmen and farmers living in the vast grasslands of the northern TP. Air pollutants from anthropogenic and natural sources can be easily transported over low bushes in the grasslands under high wind speed in north TP (Fig. S1 in the Supplement). However, fine aerosols in the troposphere have not been studied over the vast grassland in the northern TP. In this study, we collected samples at a national station of background atmospheric monitoring (NSBAM) on the top of Moshidaban Mountain of Menyuan county in Qinghai province ($37^{\circ} 35.370' \text{N}$, $101^{\circ} 17.329' \text{E}$; elevation: 3295 m), which is within the northern part of the Qinghai–Tibet Plateau (QTP) (Fig. 1). The NS-

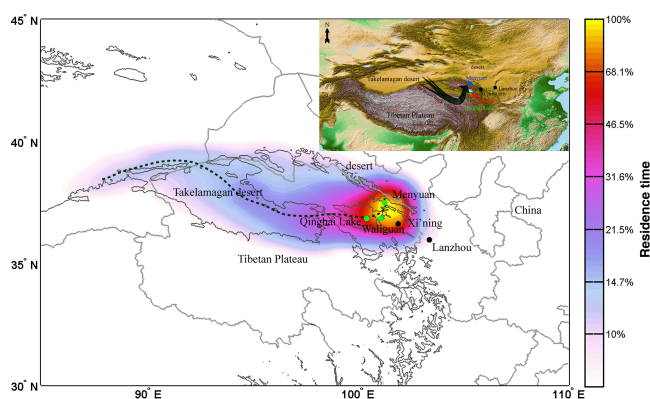


Figure 1. FLEXPART retrorplume simulations during 10 September–15 October. Topographical map showing the sampling location and surrounding regions in the Tibetan Plateau. Xining is the capital city of Qinghai province. Menyuan represents sampling site. The black line shows the major back trajectories of air mass during 10 September–15 October 2013 based on the spatial distribution of the air mass. The main air mass mainly passed through rural areas, grasslands, and desert.

BAM is 180 km north of Qinghai Lake (J. J. Li et al., 2013) and 160 km from Waliguan station (Che et al., 2011). Only a few herdsmen live in the grassland, but many agricultural activities (e.g., growing hull-less barley and rape) mainly occur around Qinghai Lake and Menyuan county.

Although many atmospheric scientists have commented on the probable aerosol impacts on climate and monsoon (Lau et al., 2006), atmospheric observations are still very limited because of the unique geographic and natural environment, electric supply problems, high maintenance costs for instruments, and lack of skilled operators. Because of the immensity of the TP, these previous studies, which are quite scattered and in diverse locations, are insufficient to adequately characterize the aerosols throughout this vast region. In addition, the mixing state of individual particles has not been examined, and only a few studies of particle types and soot have been conducted through electron microscopy (D. Zhang et al., 2001; Cong et al., 2009a). Understanding the mixing state of individual particles sheds light on their source, aging processes, and optical and hygroscopic properties (Posfai and Buseck, 2010; Li et al., 2015). In the present study, high-resolution transmission electron microscopy (TEM) is employed to study the mixing state and composition of individual submicron particles with diameters $< 1 \mu\text{m}$. The pollution levels have been evaluated and identified through continuous gaseous and particulate instruments at the sampling site. The anthropogenic sources were further identified based on particle types in the QTP.

2 Experimental methods

2.1 Aerosol sampling

Aerosol particles were collected onto copper TEM grids coated with carbon film (carbon type B, 300-mesh copper, Tianld Co., China) by a two-stage impactor with a 1 mm diameter jet nozzle and a 0.5 mm diameter jet nozzle and an air flow of 1.0 L min^{-1} . Both stages have a 50 % collection efficiency, the first at $0.80 \mu\text{m}$ and the second at $0.20 \mu\text{m}$, with an atmospheric pressure of 69 kPa, a temperature of 283.5 K, and an assumed particle density of 2 g cm^{-3} . Sampling times varied from 30 s to 15 min, depending on particle loading. After collection, each sample was placed in a sealed, dry plastic tube and stored in a desiccator at 25°C and $20 \pm 3\%$ RH to minimize exposure to ambient air and preserve it for analysis. Altogether, 70 individual samples were collected at the NABAM with the elevation at 3295 m, of which we analyzed the fine particles collected on only the second stage.

2.2 Individual particle analysis

Twenty-one aerosol particle samples collected on TEM grids were analyzed with a JEOL JEM-2100 TEM operated at 200 kV. The details about the aerosol collection were marked in Fig. 2. Elemental composition was determined semi-quantitatively by using an energy-dispersive X-ray spectrometer (EDS) that can detect elements heavier than C. Cu was excluded from the analyses because the TEM grids are made of Cu. The distribution of aerosol particles on TEM grids was not uniform, with coarser particles occurring near the center and finer particles occurring on the periphery. Therefore, to ensure that the analyzed particles were representative, five areas were chosen from the center and periphery of the sampling spot on each grid. Every particle in the selected area was analyzed. EDS spectra were collected for 15 s in order to minimize radiation exposure and potential beam damage. To better understand the properties of internally mixed aerosol particles, we also analyzed the composition of different components of individual particles, such as coatings, inclusions, and aggregations. The sampling was controlled to avoid coagulation on the substrate during sampling. The projected areas of individual particles were determined using iTEM software (Olympus Soft Imaging Solutions GmbH, Germany), the standard image analysis platform for electron microscopy. Altogether, 4218 particles in these samples were measured for statistical analyses.

2.3 Particle size measurement

Atomic force microscopy (AFM) with a tapping mode was used to analyze aerosol particles under ambient conditions. For AFM, a digital Nanoscope IIIa instrument can detect the three-dimensional morphology of particles. The AFM settings contain imaging forces between 1 and 1.5 nN, scanning rates between 0.5 and 0.8 Hz, and scanning range sizes at

$10 \mu\text{m}$ with a resolution of 512 pixels per length. After the AFM analysis, composition of the same particles was confirmed by TEM, with 194 fine aerosol particles analyzed by this method. The NanoScope analysis software can automatically obtain bearing area (A) and bearing volume (V) of each analyzed particle according to the following formula:

$$A = \pi r^2 = \pi \times \left(\frac{d}{2}\right)^2 = \frac{\pi d^2}{4} \rightarrow d = \sqrt{\frac{4A}{\pi}}, \quad (1)$$

$$V = \frac{4}{3}\pi r^3 = \frac{4}{3} \times \frac{\pi D^3}{8} = \frac{\pi D^3}{6} \rightarrow D = \sqrt[3]{\frac{6V}{\pi}}, \quad (2)$$

where d is the equivalent circle diameter (ECD) and D is the equivalent volume diameter (EVD). By plotting the ECD against the EVD (Fig. 3), we also obtain the relationship between them as $\text{EVD} = 0.64 \text{ ECD}$. As a result, ECD (d) of individual aerosol particles measured from the iTEM software can be further converted into EVD (D) based on this relationship. In this study, we only considered fine aerosol particles with equivalent volume diameter smaller than $1 \mu\text{m}$, where the correlation between the ECD and EVD is especially good (Fig. 3).

2.4 FLEXPART particle dispersion model

Air mass history was determined using the Lagrangian particle dispersion model FLEXPART (version 9.02; Stohl et al., 1998). FLEXPART simulates the release of thousands of passive tracer air parcels at the specific location, advecting them backwards in time, providing a representation of the spatial distribution of the air mass at an upwind time referred to as a “retroplume”. FLEXPART was driven with 6 h meteorology data from NCEP Climate Forecast System version 2 (NCEP-CFSv2), including land cover, temperature, relative humidity, and three-dimensional wind, in 37 levels with a resolution of $0.5^\circ \times 0.5^\circ$. In this study, the modeling periods were 72 h for each simulation, and four simulations were performed each day (beginning at 00:00, 06:00, 12:00, and 18:00, respectively) from 00:00 UTC on 10 September 2013 to 00:00 UTC on 16 October 2013. All simulations contained 10 000 particles released at the beginning over an altitude range of 3395 to 3995 m a.s.l, and the model outputs were recorded every 3 h. The output data of each simulation were combined to make Fig. 1.

2.5 $\text{PM}_{2.5}$, trace gases, BC, and meteorological measurements

A Thermo TEOM 1405 continually measured the $\text{PM}_{2.5}$ and PM_{10} particulate mass concentrations in 1 h averages. Gaseous air pollutants were measured continuously from 1 September to 15 October 2013: O_3 by a UV photometric analyzer (Teledyne Instruments, model 400EU), SO_2 by a pulsed UV fluorescence analyzer (model 100EU), CO by a non-dispersive infrared analyzer (model 300EU), and NO and NO_2 by a commercial chemiluminescence analyzer

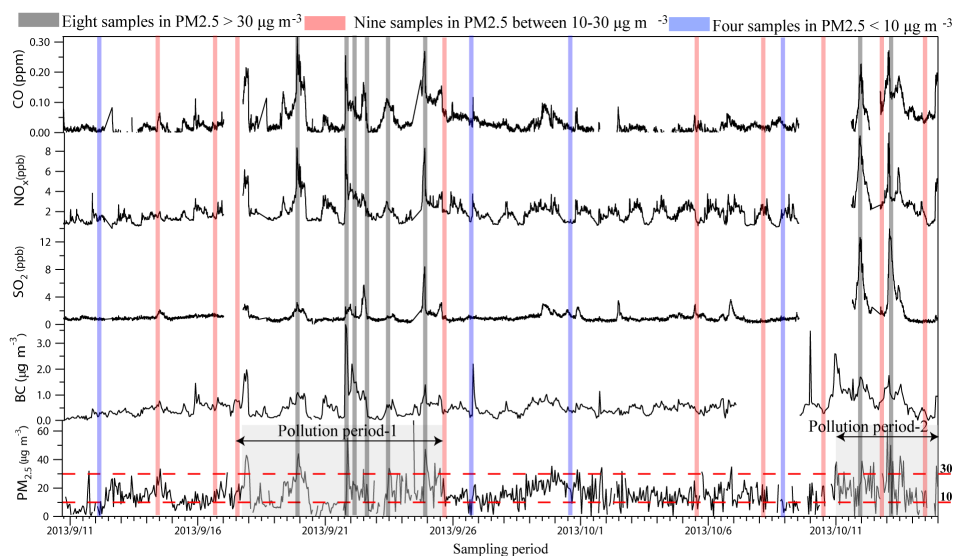


Figure 2. Time-series concentration of air pollutants (i.e., CO, NO_x, SO₂, BC, and PM_{2.5}) during 11 September–15 October 2013. The sampling time is marked by grey (PM_{2.5} ≥ 30 µg m⁻³), pink (PM_{2.5} between 10 and 30 µg m⁻³), and blue columns (PM_{2.5} < 10 µg m⁻³).

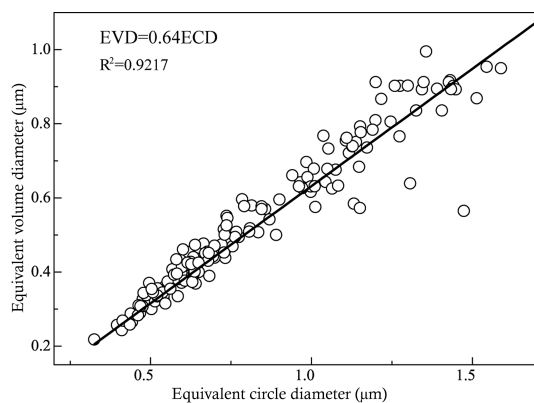


Figure 3. Correction of equivalent circle diameters (ECD) vs. equivalent volume diameter (EVD) of 194 aerosol particles.

(model 200EU), with the concentrations being recorded in 5 min averages. BC concentrations were measured by an Aethalometer and were recorded in 1 h averages. In addition, the non-refractory submicron aerosol species, including organics, sulfate, nitrate, ammonium, and chloride, were measured in situ by an Aerodyne aerosol chemical speciation monitor (ACSM) (Du et al., 2015). Wind direction, wind speed, relative humidity (RH), and temperature were measured and recorded in 1 h averages. The time-series meteorological data, shown in Fig. S1, and the PM_{2.5} and gaseous concentrations were provided by the NSBAM.

The average CO mixing ratio is 44.78 ppb at the NSBAM, much lower than the 149 ppb at Waliguan in the summer of 2006, which is the site of the observation station of the World Meteorological Organization's (WMO) Global Atmospheric Watch (GAW) (Xue et al., 2011). This contrast shows that

the NSBAM adequately represents background conditions in the expansive grasslands of the northern TP. Time-series concentration variations of six pollutants (i.e., PM_{2.5}, BC, SO₂, NO_x, CO, and O₃) show that their highest concentrations occurred from 15 to 25 September 2013, and from 11 to 15 October 2013 (Fig. 2). Therefore, we considered these two periods as typical high-pollution events. Table 1 shows that five pollutants' concentrations (i.e., PM_{2.5}, BC, SO₂, NO_x, and CO) were higher during these pollution events than in the intervening cleaner period; there was little difference in O₃ concentration among these periods. When the combustion-tracing CO and NO_x concentrations increase, O₃ mixing ratios generally decrease in the QTP due to photochemical consumption (Xue et al., 2011). The primary BC concentrations during the two pollution events were 17 and 81 % higher than the intervening cleaner period, respectively (Table 1). PM_{2.5} concentration at 17.06 µg m⁻³ at the NSBAM is slightly lower than the 21.5 µg m⁻³ in the cleaner Qinghai Lake area in the summer of 2010 (J. J. Li et al., 2013). The air mass back trajectories during the sampling period commonly came from the northwestern TP and crossed the Qinghai Lake area into the northern TP (Fig. 1). The air masses during the pollution events adequately represented highly aged and processed long-range transported aerosols in the TP. Figure 2 further displays aerosol collection time under three different PM_{2.5} levels, i.e., PM_{2.5} ≥ 30 µg m⁻³, PM_{2.5} between 10 and 30 µg m⁻³, and PM_{2.5} < 10 µg m⁻³, which represent high pollution level, medium pollution level, and a clean period.

Table 1. Concentrations of six air pollutants during the sampling period, two pollution periods, and a clean period.

Pollutants	All data		Polluted period 1		Polluted period 2		Clean period	
	mean \pm SD max, min	<i>n</i>	mean \pm SD max, min	<i>n</i>	mean \pm SD max, min	<i>n</i>	mean \pm SD max, min	<i>n</i>
PM _{2.5}	17.06 \pm 11.39 68.70, 0.20	715	17.6 \pm 11.46 59.10, 0.20	152	24.45 \pm 15.12 68.70, 0.30	99	15.32 \pm 10.41 62.80, 0.20	464
BC	0.54 \pm 0.42 3.73, 0.02	805	0.55 \pm 0.52 3.73, 0.04	176	0.85 \pm 0.50 2.04, 0.02	119	0.47 \pm 0.40 3.73, 0.03	510
SO ₂	1.27 \pm 1.34 13.93, 0.02	8822	1.2 \pm 0.99 8.43, 0.20	1981	2.73 \pm 3.09 13.93, 1.41	1063	1.03 \pm 0.65 8.43, 0.02	5778
NO _x	2.05 \pm 1.96 9.86, 0.31	8842	2.37 \pm 1.33 9.33, 0.65	2001	3.41 \pm 1.70 9.59, 0.55	1063	1.69 \pm 0.97 9.33, 0.31	5778
CO	44.78 \pm 48.03 318.00, 0.20	7822	63.45 \pm 55.59 318.00, 0.20	1939	104.23 \pm 54.69 272.40, 0.60	1030	24.68 \pm 39.91 318.00, 0.20	4853
O ₃	50 \pm 7.86 98.63, 20.43	8817	47.87 \pm 7.70 67.70, 26.66	2000	49.01 \pm 10.00 98.63, 20.43	1039	50.53 \pm 7.56 96.77, 26.66	5778

Full data period: 10 September–15 October 2013; polluted period 1: 18–25 September 2013; polluted period 2: 11–15 October 2013

3 Results

3.1 Major fine aerosol particles and mixing states

Based on elemental composition and morphology, aerosol particles were classified into six major categories: mineral dust, K–Na–Cl, fly ash, secondary inorganic aerosol (SIA) containing ammoniated sulfates and nitrates, organics, and soot (i.e., BC) (Figs. 4–5). For example, mineral dust particles normally display irregular shapes and fly ash particles are spherical, although they both have similar elemental composition, such as Si and Al. A detailed particle classification scheme is described in our previous studies (Li et al., 2014b, 2015). The nanometer-sized metal particles which have been frequently detected in ambient aerosols in East China (W. Li et al., 2013a, b) were absent in the Qinghai–Tibet plateau. Mixing properties among the six types of particles were characterized in detail. TEM observations indicate that SIA and organics coexisted in individual fine particles and that organic carbon (OC) coated (e.g., Figs. 4d and 5a), or homogeneously mixed (e.g., Fig. 6) with, these SIA particles. In other words, OC occurred on surfaces of the SIA particles. In addition, we found that many SIA–OC particles had visible inclusions such as mineral dust, fly ash, OC, and soot particles. Identification of the refractory inclusions in internally mixed particles enables one to trace particle sources and their history in the aging air mass. Their mixing properties consist mostly of SIA–soot–OC (e.g., Fig. 4c), SIA–fly ash–soot (e.g., Fig. 5d), SIA–fly ash–OC (visible) (e.g., Fig. 5d), SIA–fly ash (e.g., Fig. 5c), and SIA–mineral dust and SIA–visible OC (e.g., Fig. 5a). Therefore, SIA and OC in aerosol particles

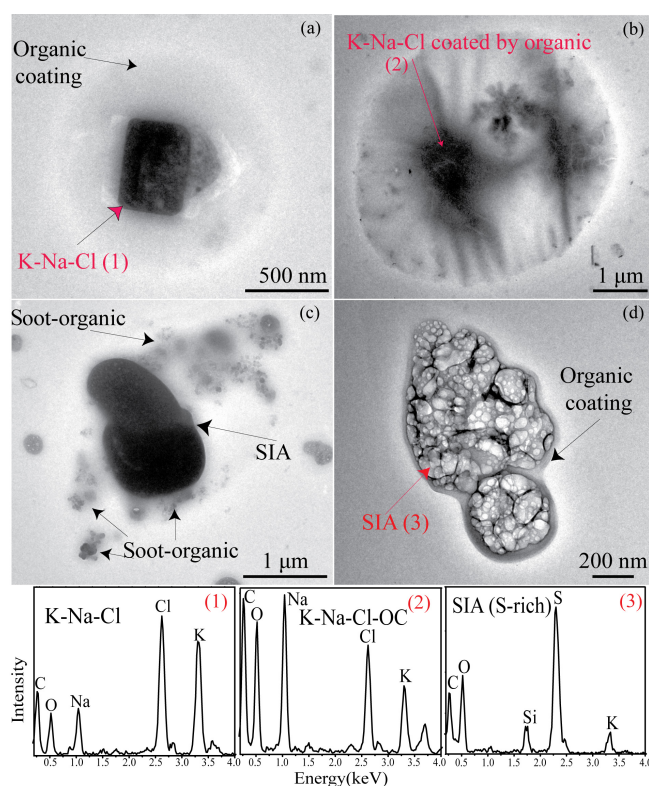


Figure 4. TEM images of a (a–b) K–Na–Cl particle with organic coating on 22 September and 13 October. (c) SIA–soot with organic coating on 22 September. (d) SIA with organic coating on 11 October. EDS spectra show elemental compositions of each particle type in each TEM image.

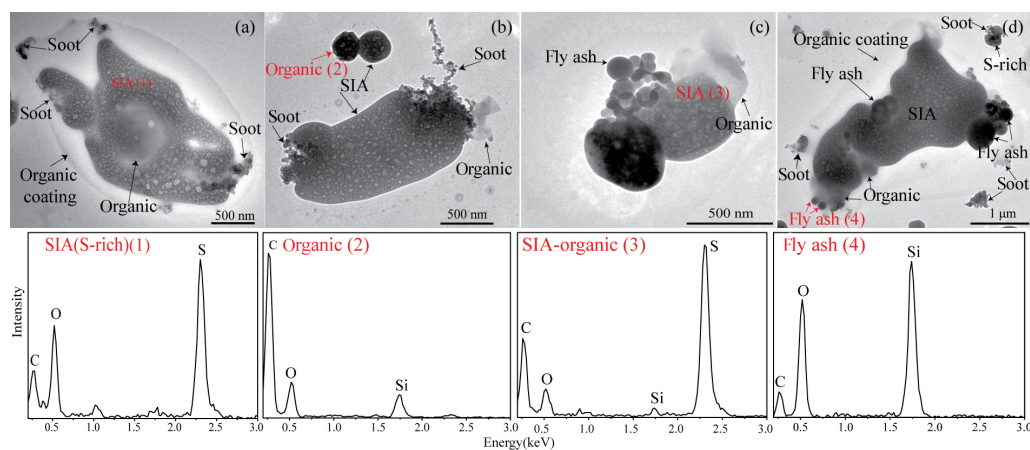


Figure 5. TEM images of (a) SIA–soot–OC (visible) with organic coating on 16 September. (b) SIA–soot–OC on 14 September. (c) SIA–fly ash–OC on 5 October. (d) SIA–fly ash–soot–OC (visible) with organic coating on 16 September. EDS spectra shows elemental composition of each particle type in each TEM image.

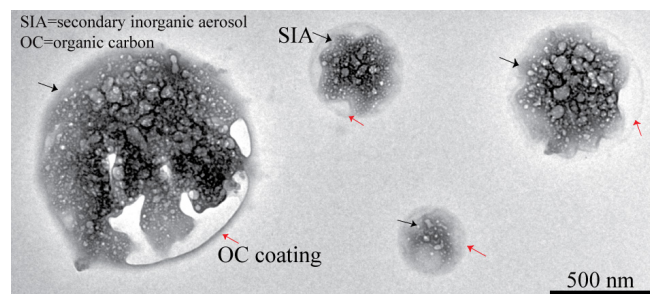


Figure 6. TEM image of individual particles collected in the clean period with $\text{PM}_{2.5}$ mass concentration less than $10 \mu\text{g m}^{-3}$. SIA particles tend to homogeneously mix with organics.

in the Qinghai–Tibet Plateau were the two most important factors for the mixing state of primary particles.

3.2 Size distribution of aerosol particles

In this section, we describe the size distribution of individual particles with their diameters from 40 nm to 1 μm at different pollution levels. The 684 particles collected during clean periods show a median diameter of 230 nm. Figure 7a shows that the size distribution of particles without inclusions determines ambient particle size.

In total, 1214 particles during high pollution levels have a median diameter of 260 nm (Fig. 7b). Particles with inclusions and particles without inclusions have median diameters of 300 and 230 nm, respectively. Figure 7b shows that particles with and without inclusions jointly determine the particle size distribution during high pollution levels. We noticed that the size distribution of inclusions in SIA displays a median diameter of 150 nm. A similar pattern of the size distribution of 2355 particles occurred at medium pollution levels (Fig. 7c). The median diameters of total individual par-

ticles, particles with inclusions, particle without inclusions, and inclusions are 290, 340, 250, and 150 nm, respectively. Therefore, the inclusions (e.g., mineral, fly ash, soot, and spherical OC particles) significantly enhanced particle sizes in the background air once they were internally mixed with sulfates.

4 Discussion

4.1 Identification of the pollution events

TEM observations show that individual particle types display large differences under three different $\text{PM}_{2.5}$ levels: $\geq 30 \mu\text{g m}^{-3}$ (high pollution level), $10\text{--}30 \mu\text{g m}^{-3}$ (medium pollution level), and $< 10 \mu\text{g m}^{-3}$ (clean period) (Fig. 3). Aerosol particles collected in clean periods mainly contained SIA and OC. Figure 6 shows that individual SIA particles were commonly coated with OC. The ACSM measurement consistently showed that SO_4^{2-} and OC were the main components in PM_1 , accounting for 33–36 and 34–48 % in mass at the sampling site, respectively (Du et al., 2015). Figure 8 presents the composition of all the analyzed individual particles at the three pollution levels. In the clean period, we found only a few anthropogenic particles such as fly ash, soot, or their mixed particles, with their contributions being less than 10 % (Fig. 8a).

The increase in KCl and soot particles is suggestive of an intense biomass burning event at the background site (Li et al., 2003). In this study, abundant K–Na–Cl particles and soot-containing particles (e.g., Fig. 4) only occurred in pollution periods 1 and 2, which have been indicated as biomass burning (Du et al., 2015). Because the K–Na–Cl particles associated with OC occurred only in the short pollution periods and are smaller than typical sea-salt or soil particles (mostly $> 1 \mu\text{m}$), it is unlikely that they originated from nat-

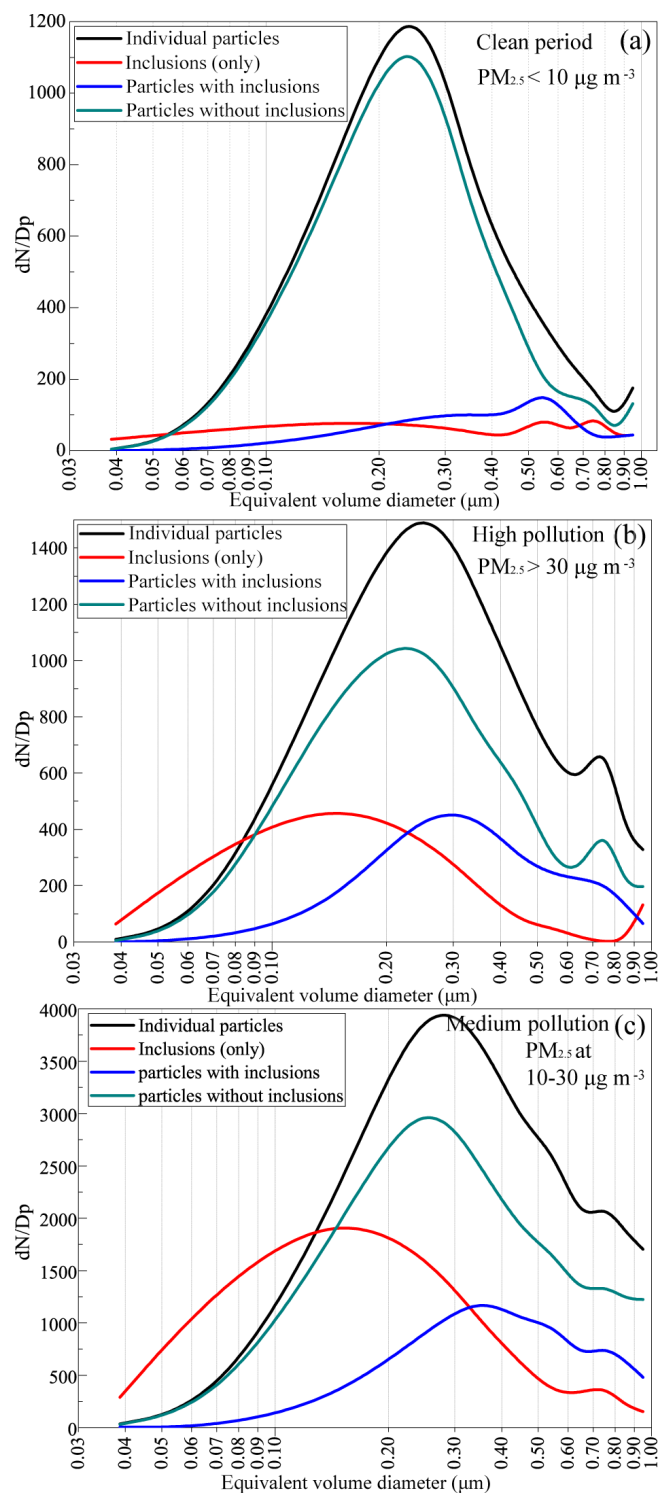


Figure 7. Size distributions of individual particles, inclusions, particles with inclusions, and particles without inclusions. (a) Clean periods under $PM_{2.5}$ at $10 \mu\text{g m}^{-3}$. (b) The high pollution level under $PM_{2.5}$ larger than $30 \mu\text{g m}^{-3}$. (c) The medium pollution level under $PM_{2.5}$ between 10 and $30 \mu\text{g m}^{-3}$.

ural sources such as saline Qinghai Lake and desert. Our field experimental investigations showed that a few farmers burned cole flowers and highland barley during the autumn harvest season, which are main season crops in the QTP. In addition, the burning of yak dung for residential heating likely caused the high $PM_{2.5}$ on 11–15 October (Du et al., 2015).

The distribution of different particle types at the medium pollution level is similar to that of the high pollution level, except for the absence of K–Na–Cl particles. Figure 8c shows that a large amount of fly-ash-containing particles occurred at the medium pollution level. Fly ash is generally considered as a reliable fingerprint of coal combustion in residential cooking, power plants, and industrial activities (Li and Shao, 2009). The fly-ash-containing particles increase from 11.40 % at the high pollution level to 21.73 % at the medium one, but soot-containing particles decrease from 38.40 to 25.87 %. This result indicates that coal combustion emissions in the QTP significantly affected the background air quality. Compared to individual particles in polluted East China, absence of nanometer-sized metal particles in the QTP suggests that there are no large heavy-metal-related industrial emissions in the area from the air mass back trajectories (Fig. 1). The China Energy Statistical Yearbook of 2013 shows that coal combustion occurs in power plants (48.5 %), heavy industries (36.4 %), and house cooking/heating in rural areas (8.6 %) in Qinghai province, particularly near the large cities such as Xining (Wen et al., 2013). Although we did not find any K–Na–Cl particle in the samples at the medium pollution level, 50 % of SIA (OC coating) and SIA–soot particles containing minor amounts of K (Fig. 4c–d) frequently occurred in the samples. During long-range transport, once coagulation and condensation of ammoniated sulfates and sulfuric acid in biomass burning particles increase, K-rich particles may transform into sulfur-rich particles with certain amounts of K (Li et al., 2014b). Therefore, SIA particles containing minor amounts of K suggest that biomass burning emissions likely contributed to the QTP aerosols on a more or less constant basis. A similar result has been obtained through the analysis of organic species in $PM_{2.5}$ at Qinghai Lake (J. J. Li et al., 2013). Therefore, we conclude that emissions from biomass burning and from coal combustion significantly contribute to the formation of anthropogenic fine particles in the atmosphere over the QTP.

4.2 Regional effects of biomass burning and industrial emissions

Previous studies have proved that trace gases such as SO_2 , NO_x , and volatile organic compounds (VOCs) from anthropogenic and natural sources had been transported over long distances in the QTP and were transformed into secondary aerosol particles (Xue et al., 2011; J. J. Li et al., 2013; Du et al., 2015; Xu et al., 2015). For example, Du et al. (2015) suggested that oxygenated organic aerosols from anthropogenic

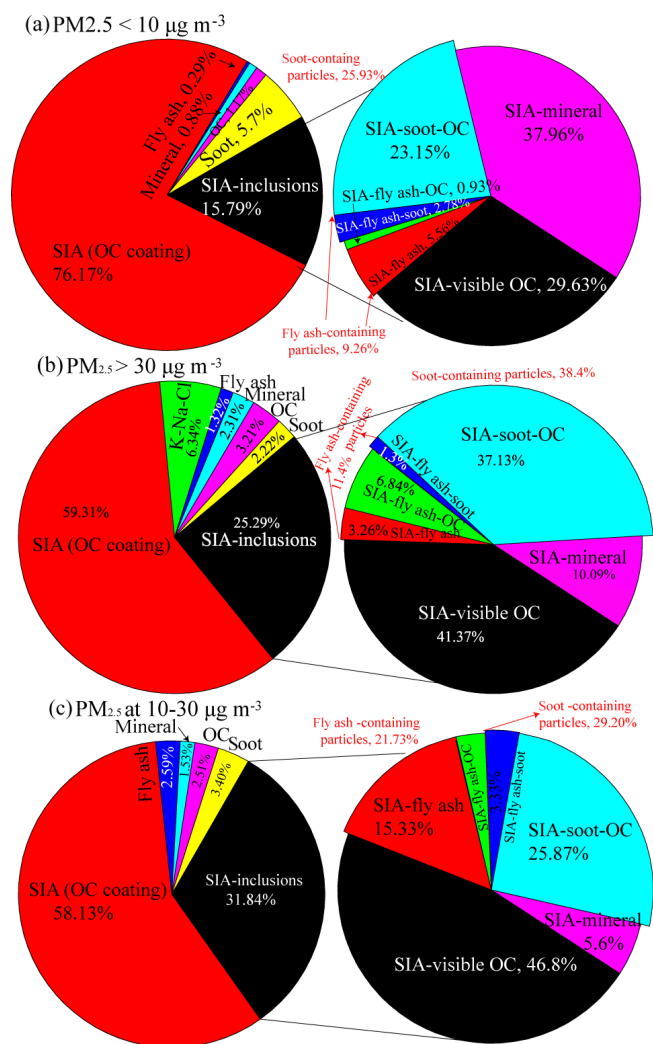


Figure 8. Identification of the pollution events based on individual particle analysis. (a) 684 individual particles (left) and 108 SIA with inclusion particles (right). (b) 1214 individual particles (left) and 307 SIA with inclusion particles (right). Eight samples were collected in $PM_{2.5}$ larger than $30 \mu g m^{-3}$ induced by biomass burning emission. (c) 2355 individual particles (left) and 750 SIA with inclusion particles (right). Nine samples were collected in $PM_{2.5}$ at the range of $10-30 \mu g m^{-3}$ induced by biomass burning and industrial emissions. Four samples were collected with $PM_{2.5}$ smaller than $10 \mu g m^{-3}$, which indicates clean period.

sources and biomass burning were transported over a long distance to the sampling site in the QTP. Because of measurement limitations, there has been no research about refractory aerosol particles (e.g., mineral, fly ash, and soot) in fine particles and primary organic particles. In contrast, TEM observations can adequately characterize these refractory particles internally mixed with SIA based on their unique morphology and composition (Figs. 4–5). We identified abundant refractory particles at the three pollution levels at the regional background site. Therefore, the nanometer-sized refractory

particles and trace gases from various anthropogenic sources including biomass burning can together be transported long distances. The FLEXPART simulation shows that these anthropogenic particles mainly originated from biomass burning between the Qinghai Lake and Menyuan county and heavy industries and coal-fired power plants in western areas of Xining (Fig. 1).

4.3 Mixing mechanisms of aged aerosol particles

In this study, an individual particle clearly containing more than two types of aerosol components (e.g., mineral dust, K–Na–Cl, fly ash, SIA, organics, and soot) has been defined as an aged particle. More than 90 % of particles at the background site were highly aged. SIA particles with OC coating were the dominant particles and could determine the hygroscopic properties of the ambient aerosol particles. OC coatings on inorganic particles can induce an early deliquescence of particle surface compared to that of the pure inorganic compounds (Li et al., 2014a). Recently, Mikhailov et al. (2015) found that the semi-solid state of the OC coating can lead to kinetic limitations of water uptake and release during hydration and dehydration cycles in the background area. OC dominated in fine particles, accounting for 43 % of mass on average, followed by sulfate (28 %) and nitrate (1 %) (Du et al., 2015). TEM observations further indicated that OC can be heterogeneously and homogeneously mixed with all the fine SIA particles (Figs. 6, 9–10). This finding is in agreement with the study of new particle formation and growth events during the sampling period, in which oxygenated organics significantly contributed into particle growth in the QTP (Du et al., 2015). SIA particles with OC coating (i.e., particle without inclusions in Fig. 7) shift to a smaller particle size than the total individual particles. Gas condensation on the existing particles is an important chemical process for formation of SIA with OC coating. Therefore, OC coating of the aged aerosol particles is likely an important factor to determine particle hygroscopic growth and phase transitions in the QTP.

Inclusions within SIA particles increase their size by 36–42 % (Fig. 7). The size distribution of individual particles shows that particles without inclusions have a median size of 200–250 nm at the background site. Figure 7 shows that the number of particles with inclusions increases substantially with diameters above 200 nm. In addition, Figs. 9–10 show that soot, fly ash, and visible OC particles likely adhere to the surface of SIA particles, which is different from many refractory particles embedded within SIA particles in East China (Li and Shao, 2009; W. J. Li et al., 2011; Li et al., 2014b). Therefore, the coagulation process between primary refractory particles and SIA particles with diameters > 200 nm could be dominant in the atmosphere. The results are different from the background aerosol particles in Siberia, where these soot, fly ash, and visible OC particles are absent (Mikhailov et al., 2015). In particular, the mixing structure

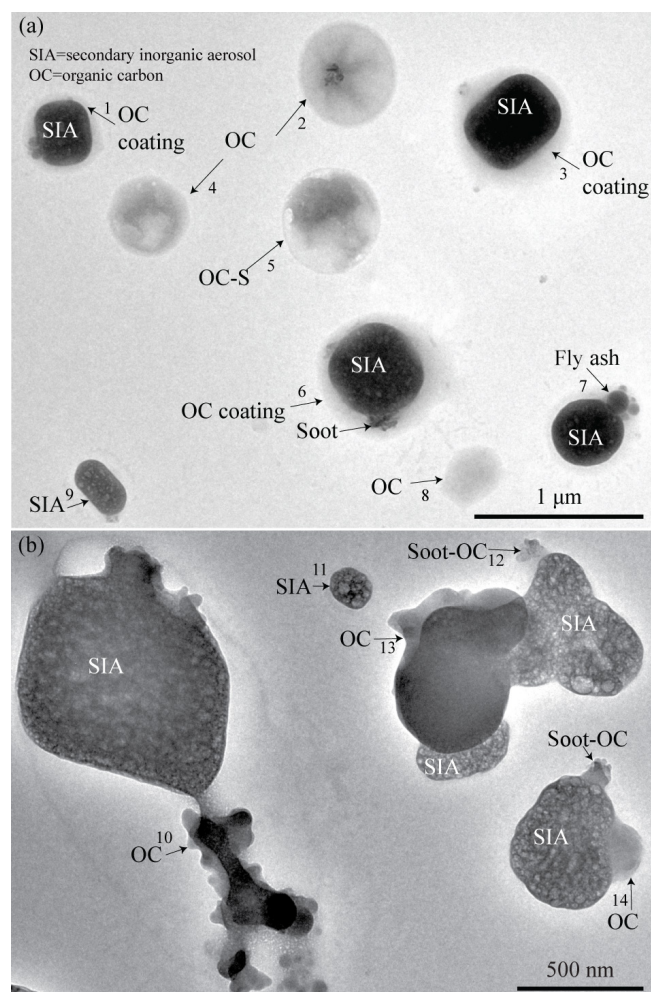


Figure 9. Individual particles during biomass burning periods with $\text{PM}_{2.5}$ mass concentration larger than $30 \mu\text{g m}^{-3}$. (a) OC and SIA–soot–OC coating particles on 12 October. (b) SIA–soot–visible OC on 19 October. OC in particles 1, 3, 6, 10, 13, and 14 are heterogeneously mixed with SIA particles and particles 2, 4, 5, and 8 homogeneously mixed with minor SIA.

of soot on the surface of SIA particles is different from previous studies (Li et al., 2003; Adachi et al., 2010; Li et al., 2015). Therefore, sulfates cannot act as the lens to enhance optical absorption of soot particles before individual particles completely deliquesce in humid air (Ramanathan and Carmichael, 2008). Light absorption of soot on surfaces of sulfate particles is 30 % lower than soot centered within sulfate particles (Adachi et al., 2010). We found that the number of soot-containing particles increases during the biomass burning periods (Fig. 8b–c). Also, Fig. 3 shows that the BC concentrations exceeded $1.0 \mu\text{g m}^{-3}$ during biomass burning periods, which is 2 times higher than the average value during the sampling period. As a result, large numbers of soot particles from biomass burning in background atmosphere likely change atmospheric optical absorption and modify op-

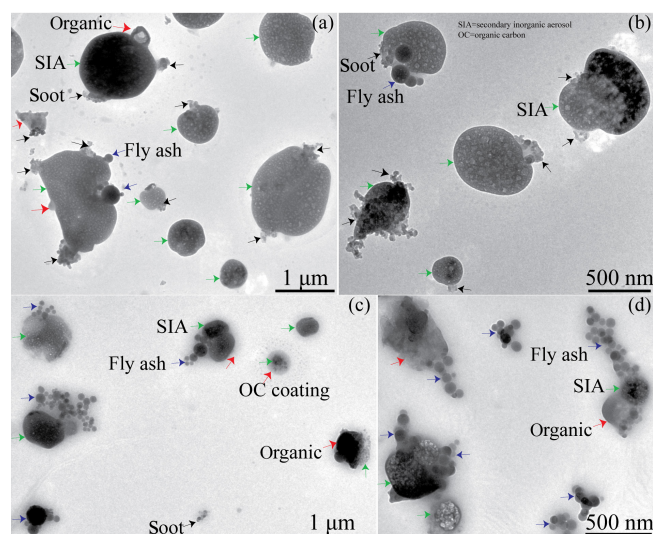


Figure 10. Individual particles collected under $\text{PM}_{2.5}$ mass concentration among $10\text{--}30 \mu\text{g m}^{-3}$. (a) Mixture of SIA and soot, fly ash particles collected on 14 September. (b) Mixture of SIA and soot, fly ash particles collected on 18 September. (c) Mixture of SIA and fly ash, soot, organics collected on 29 September. (d) Mixture of SIA and fly ash, soot, organics collected on 10 October. Organics are heterogeneously mixed with SIA.

tical feedback of ice/snow after their deposition in the QTP (Che et al., 2011; Ming et al., 2012). The microstructure of soot particles can improve understanding of the optical properties of fine aerosol particles and allow for better evaluation of their climate impacts using climate models.

TEM observations reveal distinct rims on some larger particles, as the examples shown in Figs. 5a, 5d, 9b, and 10a. Our previous studies showed that the cloud and fog residues on the substrate can display distinct rims (Kojima et al., 2004; W. Li et al., 2011; W. J. Li, 2011). Therefore, these large particles with distinct rims probably undergo complicated atmospheric transformation such as cloud/fog processing during their growth. Briefly, our study indicates that aerosol particles in different size regimes have different atmospheric chemical or physical processes in the background air over the QTP.

4.4 Further considerations about fine particles over the Qinghai–Tibetan Plateau

Emissions from coal combustion and biomass burning contribute fine particles into the background air over the QTP. Because the complex aerosol particles from different anthropogenic sources intruded into pristine background air, the suspended aerosols became highly aged. Because of the sensitive feedback of climate in the TP, these aged aerosol particles in the plateau become particularly interesting. Firstly, transport and sources of aerosol particles should be evaluated, and, indeed, most studies in the TP have accomplished

this (Cong et al., 2009a, b; Engling et al., 2011; Lu et al., 2012; Du et al., 2015; Xu et al., 2015). These studies all suggested that fine particles from biomass burning and other anthropogenic sources (cooking and vehicular emissions) often arrived at the TP through long-range transport. However, the emissions of coal combustion from power plants or other industrial sources have a decidedly regional influence. This has not been reported yet. Our studies provide new evidence that fly ash particles serve as a reliable fingerprint of coal combustion at the background site. Following economic development in western China, coal combustion has increased, chiefly for electrical power generation and other industrial activities (Fig. S2). Secondly, highly aged particles such as ambient aerosols and CCN in the atmosphere and sediment in ice/snow can directly or indirectly impact on climate in the TP (Cong et al., 2009b; You et al., 2010; Che et al., 2011; Lu et al., 2012; Ming et al., 2012; He et al., 2014; Wang et al., 2015; Yang et al., 2015). At the background sampling site the mean BC concentration was $0.54 \mu\text{g m}^{-3}$. Interestingly, we found that most fine soot (BC) particles adhere to individual SIA particles (Figs. 9–10) in the Qinghai Plateau, while many soot particles were embedded within SIA in polluted areas of East China (Li and Shao, 2009; W. J. Li et al., 2011). The physical properties (e.g., mixing structure and size) of soot in air and ice/snow should be further studied in detail in the TP, as this could help to improve current climate models. Thirdly, fine aerosol particles in the TP mainly contain OC and sulfates with minor amounts of nitrates. The result is largely different from fine particles with high nitrate in more polluted areas (J. J. Li et al., 2013; Du et al., 2015; Xu et al., 2015). Although regional transport from anthropogenic sources or biomass burning significantly increases particle concentrations, mineral dust from surrounding deserts and organics from plants are still dominant in the TP throughout the year (X. Y. Zhang et al., 2001; Wang et al., 2010; J. J. Li et al., 2013; Xu et al., 2014).

5 Conclusions

Time series of six pollutants ($\text{PM}_{2.5}$, BC, SO_2 , NO_x , CO, and O_3) were obtained at a national station of background atmospheric monitoring (NSBAM) on the top of Moshidaban Mountain in the northern QTP during 15 September–15 October 2013. The mean concentrations of $\text{PM}_{2.5}$, BC, SO_2 , NO_x , CO, and O_3 were $17.06 \mu\text{g m}^{-3}$, $0.54 \mu\text{g m}^{-3}$, 1.27 ppb, 2.05 ppb, 44.78 ppb, and 50.00 ppb, respectively. TEM was employed to study individual fine particles with diameters less than $1 \mu\text{m}$ that were classified into six major particle types: mineral dust, K–Na–Cl, fly ash, secondary inorganic aerosol (SIA) containing ammoniated sulfates and nitrates, organics, and soot (i.e., BC). Individual fine particle types display large differences at three different $\text{PM}_{2.5}$ levels: $\text{PM}_{2.5} \geq 30 \mu\text{g m}^{-3}$ (high pollution level), $\text{PM}_{2.5} 10\text{--}30 \mu\text{g m}^{-3}$ (medium pollution level), and $< 10 \mu\text{g m}^{-3}$ (clean

period). Individual fine particles in clean periods mainly contained SIA and organics. The presence of K–Na–Cl coated by organics and increased soot particles during high pollution levels suggests an intense biomass burning event near the background site. Large numbers of fly-ash-containing particles occurred at the medium pollution level. The fly-ash-containing particles increased from 11.40 % at the medium pollution level to 21.73 % at the high pollution level, but soot-containing particles decreased from 38.40 to 25.87 %. This result indicates that coal combustion emissions in the QTP significantly affected the background air quality. In addition, SIA particles containing minor amounts of K suggest that biomass burning emissions were a constant contributor to aerosol particles in the QTP. We concluded that the emissions from biomass burning and anthropogenic activities relating to coal consumption contribute anthropogenic particles into the QTP atmosphere.

Aerosol particles containing an SIA core and OC coating display smaller median size than the total particles. Gas condensation on the particles is an important chemical process for their formation. The number concentration of particles with inclusions increased markedly above 200 nm. TEM observations show that refractory aerosols (e.g., soot, fly ash, and visible organic particles) likely adhere to the surface of SIA particles, suggesting physical coagulation could be dominant in background air. These results notably improve our understanding of sources and aging processes of long-range transported aerosols in the QTP. The transport of these aerosol particles, as well as their hygroscopic and optical properties and atmospheric chemistry, requires further study in the TP.

The Supplement related to this article is available online at doi:10.5194/acp-15-13365-2015-supplement.

Author contributions. W. J. Li and J. M. Chen designed the research and wrote the paper; W. J. Li and S. R. Chen carried out TEM and AFM experiments; Y. S. Xu, X. C. Guo, Y. L. Sun, and X. Y. Yang conducted field experiments; X. D. Zhao provided the online monitoring data; Y. S. Xu, J. M. Chen, Z. F. Wang, and W. X. Wang led the projects.

Acknowledgements. We appreciate Peter Hyde's comments and proofreading. We are grateful to Yong Ren for processing FLEX-PART data for Fig. 1. This work was supported by the National Natural Science Foundation of China (41575116 and 41375133), the Shandong Provincial Science Fund for Distinguished Young Scholars (JQ201413), the Young Scholars Program of Shandong University (2015WLJH37), Taishan Scholars (ts20120522), the Fundamental Research Funds of Shandong University (2014QY001), and the State Key Laboratory of Atmospheric

Boundary Layer Physics and Atmospheric Chemistry (LAPC-KF-2014-03).

Edited by: T. Wang

References

- Adachi, K., Chung, S. H., and Buseck, P. R.: Shapes of soot aerosol particles and implications for their effects on climate, *J. Geophys. Res.*, 115, D15206, doi:10.1029/2009JD012868, 2010.
- Cao, J., Tie, X., Xu, B., Zhao, Z., Zhu, C., Li, G., and Liu, S.: Measuring and modeling black carbon (BC) contamination in the SE Tibetan Plateau, *J. Atmos. Chem.*, 67, 45–60, 2010.
- Che, H., Wang, Y., and Sun, J.: Aerosol optical properties at Mt. Waliguan Observatory, China, *Atmos. Environ.*, 45, 6004–6009, 2011.
- Cong, Z., Kang, S., Dong, S., and Zhang, Y.: Individual particle analysis of atmospheric aerosols at Nam Co, Tibetan Plateau, *Aerosol Air Qual. Res.*, 9, 323–331, 2009a.
- Cong, Z., Kang, S., Smirnov, A., and Holben, B.: Aerosol optical properties at Nam Co, a remote site in central Tibetan Plateau, *Atmos. Res.*, 92, 42–48, 2009b.
- Cong, Z., Kawamura, K., Kang, S., and Fu, P.: Penetration of biomass-burning emissions from South Asia through the Himalayas: new insights from atmospheric organic acids, *Sci. Rep.*, 5, 9580, doi:10.1038/srep09580, 2015.
- Du, W., Sun, Y. L., Xu, Y. S., Jiang, Q., Wang, Q. Q., Yang, W., Wang, F., Bai, Z. P., Zhao, X. D., and Yang, Y. C.: Chemical characterization of submicron aerosol and particle growth events at a national background site (3295 m a.s.l.) on the Tibetan Plateau, *Atmos. Chem. Phys.*, 15, 10811–10824, doi:10.5194/acp-15-10811-2015, 2015.
- Duo, B., Zhang, Y., Kong, L., Fu, H., Hu, Y., Chen, J., Li, L., and Qiong, A.: Individual particle analysis of aerosols collected at Lhasa City in the Tibetan Plateau, *J. Environ. Sci.*, 29, 165–177, 2015.
- Engling, G., Zhang, Y.-N., Chan, C.-Y., Sang, X.-F., Lin, M., Ho, K.-F., Li, Y.-S., Lin, C.-Y., and Lee, J. J.: Characterization and sources of aerosol particles over the southeastern Tibetan Plateau during the Southeast Asia biomass-burning season, *Tellus B*, 63, 117–128, doi:10.1111/j.1600-0889.2010.00512.x, 2011.
- He, C., Li, Q., Liou, K.-N., Takano, Y., Gu, Y., Qi, L., Mao, Y., and Leung, L. R.: Black carbon radiative forcing over the Tibetan Plateau, *Geophys. Res. Lett.*, 41, 7806–7813, 2014.
- Kojima, T., Buseck, P. R., Wilson, J. C., Reeves, J. M., and Mahoney, M. J.: Aerosol particles from tropical convective systems: Cloud tops and cirrus anvils, *J. Geophys. Res.*, 109, 12201–12201, 2004.
- Kopacz, M., Mauzerall, D. L., Wang, J., Leibensperger, E. M., Henze, D. K., and Singh, K.: Origin and radiative forcing of black carbon transported to the Himalayas and Tibetan Plateau, *Atmos. Chem. Phys.*, 11, 2837–2852, doi:10.5194/acp-11-2837-2011, 2011.
- Lau, K. M., Kim, M. K., and Kim, K. M.: Asian summer monsoon anomalies induced by aerosol direct forcing: the role of the Tibetan Plateau, *Clim. Dynam.*, 26, 855–864, 2006.
- Li, C., Kang, S., Zhang, Q., and Kaspari, S.: Major ionic composition of precipitation in the Nam Co region, Central Tibetan Plateau, *Atmos. Res.*, 85, 351–360, 2007.
- Li, J., Posfai, M., Hobbs, P. V., and Buseck, P. R.: Individual aerosol particles from biomass burning in southern Africa: 2, Compositions and aging of inorganic particles, *J. Geophys. Res.*, 108, 8384, doi:10.1029/2002JD002310, 2003.
- Li, J. J., Wang, G. H., Wang, X. M., Cao, J. J., Sun, T., Cheng, C. L., Meng, J. J., Hu, T. F., and Liu, S. X.: Abundance, composition and source of atmospheric PM 2.5 at a remote site in the Tibetan Plateau, China, *Tellus B*, 65, 20130027, doi:10.3402/tellusb.v65i0.20281, 2013.
- Li, W., Li, P., Sun, G., Zhou, S., Yuan, Q., and Wang, W.: Cloud residues and interstitial aerosols from non-precipitating clouds over an industrial and urban area in northern China, *Atmos. Environ.*, 45, 2488–2495, 2011.
- Li, W., Wang, T., Zhou, S., Lee, S., Huang, Y., Gao, Y., and Wang, W.: Microscopic Observation of Metal-Containing Particles from Chinese Continental Outflow Observed from a Non-Industrial Site, *Environ. Sci. Technol.*, 47, 9124–9131, 2013a.
- Li, W., Wang, Y., Collett, J. L., Chen, J., Zhang, X., Wang, Z., and Wang, W.: Microscopic Evaluation of Trace Metals in Cloud Droplets in an Acid Precipitation Region, *Environ. Sci. Technol.*, 47, 4172–4180, 2013b.
- Li, W., Chi, J., Shi, Z., Wang, X., Chen, B., Wang, Y., Li, T., Chen, J., Zhang, D., Wang, Z., Shi, C., Liu, L., and Wang, W.: Composition and hygroscopicity of aerosol particles at Mt. Lu in South China: Implications for acid precipitation, *Atmos. Environ.*, 94, 626–636, doi:10.1016/j.atmosenv.2014.06.003, 2014a.
- Li, W., Shao, L., Shi, Z., Chen, J., Yang, L., Yuan, Q., Yan, C., Zhang, X., Wang, Y., Sun, J., Zhang, Y., Shen, X., Wang, Z., and Wang, W.: Mixing state and hygroscopicity of dust and haze particles before leaving Asian continent, *J. Geophys. Res.*, 119, 1044–1059, 2014b.
- Li, W., Shao, L., Zhang, D., Ro, C.-U., Hu, M., Bi, X., Geng, H., Matsuki, A., Niu, H., and Chen, J.: A review of single aerosol particle studies in the atmosphere of East Asia: morphology, mixing state, source, and heterogeneous reactions, *J. Clean. Prod.*, doi:10.1016/j.jclepro.2015.04.050, in press, 2015.
- Li, W. J. and Shao, L. Y.: Transmission electron microscopy study of aerosol particles from the brown hazes in northern China, *J. Geophys. Res.*, 114, D09302, doi:10.1029/2008JD011285, 2009.
- Li, W. J., Zhou, S. Z., Wang, X. F., Xu, Z., Yuan, C., Yu, Y. C., Zhang, Q. Z., and Wang, W. X.: Integrated evaluation of aerosols from regional brown hazes over northern China in winter: Concentrations, sources, transformation, and mixing states, *J. Geophys. Res.*, 116, d09301, doi:10.1029/2010JD015099, 2011.
- Lu, Z., Streets, D. G., Zhang, Q., and Wang, S.: A novel back-trajectory analysis of the origin of black carbon transported to the Himalayas and Tibetan Plateau during 1996–2010, *Geophys. Res. Lett.*, 39, L01809, doi:10.1029/2011gl049903, 2012.
- Mikhailov, E. F., Mironov, G. N., Pöhlker, C., Chi, X., Krüger, M. L., Shiraiwa, M., Förster, J.-D., Pöschl, U., Vlasenko, S. S., Ryskhovich, T. I., Weigand, M., Kilcoyne, A. L. D., and Andreae, M. O.: Chemical composition, microstructure, and hygroscopic properties of aerosol particles at the Zotino Tall Tower Observatory (ZOTTO), Siberia, during a summer campaign, *Atmos. Chem. Phys.*, 15, 8847–8869, doi:10.5194/acp-15-8847-2015, 2015.

- Ming, J., Du, Z., Xiao, C., Xu, X., and Zhang, D.: Darkening of the mid-Himalaya glaciers since 2000 and the potential causes, *Environ. Res. Lett.*, 7, 014021, doi:10.1088/1748-9326/7/1/014021, 2012.
- Posfai, M. and Buseck, P. R.: Nature and Climate Effects of Individual Tropospheric Aerosol Particles, *Annu. Rev. Earth Pl. Sc.*, 38, 17–43, 2010.
- Ramanathan, V. and Carmichael, G.: Global and regional climate changes due to black carbon, *Nat. Geosci.*, 1, 221–227, 2008.
- Stohl, A., Hittenberger, M., and Wotawa, G.: Validation of the Lagrangian particle dispersion model FLEXPART against large-scale tracer experiment data, *Atmos. Environ.*, 32, 4245–4264, doi:10.1016/S1352-2310(98)00184-8, 1998.
- Wang, Q. Y., Huang, R.-J., Cao, J. J., Tie, X. X., Ni, H. Y., Zhou, Y. Q., Han, Y. M., Hu, T. F., Zhu, C. S., Feng, T., Li, N., and Li, J. D.: Black carbon aerosol in winter northeastern Qinghai-Tibetan Plateau, China: the effects from South Asia pollution, *Atmos. Chem. Phys. Discuss.*, 15, 14141–14169, doi:10.5194/acpd-15-14141-2015, 2015.
- Wang, X., Huang, J., Zhang, R., Chen, B., and Bi, J.: Surface measurements of aerosol properties over northwest China during ARM China 2008 deployment, *J. Geophys. Res.*, 115, D00k27, doi:10.1029/2009JD013467, 2010.
- Wen, J., Meng, H., and Wang, X.: China Energy Statistical Yearbook, Department of Energy Statistics, National Bureau of Statistics, People's Republic of China, Beijing, 1–355, 2013.
- Xia, X., Zong, X., Cong, Z., Chen, H., Kang, S., and Wang, P.: Base-line continental aerosol over the central Tibetan plateau and a case study of aerosol transport from South Asia, *Atmos. Environ.*, 45, 7370–7378, 2011.
- Xu, B., Cao, J., Hansen, J., Yao, T., Joswita, D. R., Wang, N., Wu, G., Wang, M., Zhao, H., Yang, W., Liu, X., and He, J.: Black soot and the survival of Tibetan glaciers, *Proc. Natl. Acad. Sci. USA*, 106, 22114–22118, 2009.
- Xu, J., Zhang, Q., Li, X., Ge, X., Xiao, C., Ren, J., and Qin, D.: Dissolved Organic Matter and Inorganic Ions in a Central Himalayan Glacier – Insights into Chemical Composition and Atmospheric Sources, *Environ. Sci. Technol.*, 47, 6181–6188, 2013.
- Xu, J., Wang, Z., Yu, G., Qin, X., Ren, J., and Qin, D.: Characteristics of water soluble ionic species in fine particles from a high altitude site on the northern boundary of Tibetan Plateau: Mixture of mineral dust and anthropogenic aerosol, *Atmos. Res.*, 143, 43–56, 2014.
- Xu, J. Z., Zhang, Q., Wang, Z. B., Yu, G. M., Ge, X. L., and Qin, X.: Chemical composition and size distribution of summertime PM_{2.5} at a high altitude remote location in the northeast of the Qinghai–Xizang (Tibet) Plateau: insights into aerosol sources and processing in free troposphere, *Atmos. Chem. Phys.*, 15, 5069–5081, doi:10.5194/acp-15-5069-2015, 2015.
- Xue, L. K., Wang, T., Zhang, J. M., Zhang, X. C., Deliger, Poon, C. N., Ding, A. J., Zhou, X. H., Wu, W. S., Tang, J., Zhang, Q. Z., and Wang, W. X.: Source of surface ozone and reactive nitrogen speciation at Mount Waliguan in western China: New insights from the 2006 summer study, *J. Geophys. Res.*, 116, D07306, doi:10.1029/2010JD014735, 2011.
- Yang, S., Xu, B., Cao, J., Zender, C. S., and Wang, M.: Climate effect of black carbon aerosol in a Tibetan Plateau glacier, *Atmos. Environ.*, 111, 71–78, 2015.
- You, Q., Kang, S., Flügel, W.-A., Sanchez-Lorenzo, A., Yan, Y., Huang, J., and Martin-Vide, J.: From brightening to dimming in sunshine duration over the eastern and central Tibetan Plateau (1961–2005), *Theor. Appl. Climatol.*, 101, 445–457, 2010.
- Zhang, D., Iwasaka, Y., and Shi, G.: Soot particles and their impacts on the mass cycle in the Tibetan atmosphere, *Atmos. Environ.*, 35, 5883–5894, 2001.
- Zhang, X. Y., Arimoto, R., Cao, J. J., An, Z. S., and Wang, D.: Atmospheric dust aerosol over the Tibetan Plateau, *J. Geophys. Res.*, 106, 18471–18476, 2001.
- Zhao, Z., Cao, J., Shen, Z., Xu, B., Zhu, C., Chen, L. W. A., Su, X., Liu, S., Han, Y., Wang, G., and Ho, K.: Aerosol particles at a high-altitude site on the Southeast Tibetan Plateau, China: Implications for pollution transport from South Asia, *J. Geophys. Res.*, 118, 11360–11375, 2013.
- Zheng, W., Yao, T., Joswiak, D. R., Xu, B., Wang, N., and Zhao, H.: Major ions composition records from a shallow ice core on Mt. Tanggula in the central Qinghai-Tibetan Plateau, *Atmos. Res.*, 97, 70–79, 2010.